

# COSMOGLOBE DR2. V. Spatial correlations between thermal dust and ionized carbon emission in *Planck* HFI and COBE-DIRBE

E. Gjerløw<sup>1\*</sup>, R. M. Sullivan<sup>1</sup>, R. Aurvik<sup>1</sup>, A. Basyrov<sup>1</sup>, L. A. Bianchi<sup>1</sup>, A. Bonato<sup>2</sup>, M. Brilenkov<sup>1</sup>, H. K. Eriksen<sup>1</sup>, U. Fuskeland<sup>1</sup>, M. Galloway<sup>1</sup>, K. A. Glasscock<sup>1</sup>, L. T. Hergt<sup>3</sup>, D. Herman<sup>1</sup>, J. G. S. Lunde<sup>1</sup>, M. San<sup>1</sup>, A. I. Silva Martins<sup>1</sup>, D. Sponseller<sup>4</sup>, N.-O. Stutz<sup>1</sup>, H. Thommesen<sup>1</sup>, V. Vikenes<sup>1</sup>, D. J. Watts<sup>1</sup>, I. K. Wehus<sup>1</sup>, and L. Zapelli<sup>2,5,6</sup>

<sup>1</sup> Institute of Theoretical Astrophysics, University of Oslo, Blindern, Oslo, Norway

<sup>2</sup> Dipartimento di Fisica, Università degli Studi di Milano, Via Celoria, 16, Milano, Italy

<sup>3</sup> Department of Physics and Astronomy, University of British Columbia, 6224 Agricultural Road, Vancouver BC, V6T1Z1, Canada

<sup>4</sup> Department of Space, Earth and Environment, Chalmers University of Technology, Gothenburg, Sweden

<sup>5</sup> Università di Trento, Università degli Studi di Milano, CUP E66E23000110001

<sup>6</sup> INFN sezione di Milano, 20133 Milano, Italy

January 12, 2026

## ABSTRACT

We fit five tracers of thermal dust emission to ten *Planck* HFI and COBE-DIRBE frequency maps between 353 GHz and 25 THz, aiming to map the relative importance of each physical host environment as a function of frequency and position on the sky. Four of these correspond to classic thermal dust tracers, namely H I (HI4PI), CO (Dame et al. 2001a), H $\alpha$  (WHAM, Haffner et al. (2003a, 2016)), and dust extinction (*Gaia*; Edenhofer et al. 2024), while the fifth is ionized carbon (C II) emission as observed by COBE-FIRAS. To our knowledge, this has until now been considered to be primarily a gas tracer, rather than a dust tracer. After smoothing all data to the common resolution of the FIRAS experiment, and subtracting subdominant astrophysical components as appropriate for each channel (cosmic microwave and infrared backgrounds, and zodiacal light), we jointly fit these five templates to each frequency channel through standard multi-variate linear regression. At frequencies higher than 1 THz, we find that the dominant tracer is in fact C II, and above 10 THz this component accounts for almost the entire fitted signal; at frequencies below 1 THz, its importance is second only to H I. We further find that all five components are well described by a modified blackbody spectral energy density (SED) up to some component-dependent maximum frequency ranging between 1 and 5 THz. In this interpretation, the C II-correlated component is the hottest among all five with an effective temperature of about 25 K. For comparison, the H I and CO components have effective temperatures of 16 K and 12 K, respectively. The H $\alpha$  component has a temperature of 18 K, and, unlike the other four, is observed in absorption rather than emission. The spectral indices of the five components range between  $\beta = 1.4$  (for H I) and 2.6 (for H $\alpha$ ); for the C II component,  $\beta = 1.56$ . Despite the simplicity of this model, which relies only external templates coupled to spatially isotropic SEDs, we find that it captures 98 % of the full signal root mean squared (RMS) below 1 THz. At higher frequencies, which are more susceptible to non-thermal emission processes, the model still captures more than 80 % of the full signal RMS. This high efficiency suggests that spatial variations in the thermal dust SED, as for instance reported by *Planck* and other experiments, may be more economically modelled on large angular scales in terms of a spatial mixing of individually isotropic physical components, than by a single uniform well-mixed interstellar medium coupled to a spatially varying temperature field, as has been the norm until now. Indeed, the results found in this paper motivate the thermal dust model adopted for the COSMOGLOBE DR2 re-analysis of the COBE-DIRBE data, and we believe that they may also provide inspiration for refining both current theoretical interstellar medium models and component separation algorithms in general.

**Key words.** ISM: general - Zodiacal dust, Interplanetary medium - Cosmology: observations, diffuse radiation - Galaxy: general

## 1. Introduction

The interstellar medium (ISM) plays a ubiquitous role in modern astrophysics and cosmology across the electromagnetic spectrum (e.g., Draine 2011, Hensley & Draine 2023). On one hand, understanding the composition and physics of the ISM informs us about the structure and dynamics of both the Milky Way and distant galaxies, and ISM studies are therefore an important and interesting field of astronomy in their own right. On the other hand, ISM radiation is a key contaminant for a broad range of other high-impact science targets, for instance the search for gravitational waves in the cosmic microwave background (CMB), dark matter annihilation in gamma-ray observations, or

dark energy constraints through high-precision measurements of distant supernovae. Accurate ISM modelling is therefore a key aspect in 21st century astrophysics.

Broadly speaking, the ISM is comprised of cosmic rays (relativistic particles), gas (atoms or small molecules), and dust (large molecules, typically ranging in size from a few angstroms to 100  $\mu\text{m}$ ). All of these emit electromagnetic radiation at various frequencies, for instance through synchrotron, bremsstrahlung, quantum mechanical line emission, or thermal emission. In addition, dust grains absorb electromagnetic radiation with wavelengths that are comparable to the grain size, which due to the grain distribution happens most notably in wavelengths ranging from infrared to X-rays.

The current paper is part of a suite of seven companion papers that describes the COSMOGLOBE Data Release 2 (DR2; Watts

\* Corresponding author: E. Gjerløw; [eirik.gjerlow@astro.uio.no](mailto:eirik.gjerlow@astro.uio.no)

et al. 2024a). The primary main goal of this work is to reanalyze the *COBE*-DIRBE data (Hauser et al. 1998) within a global Bayesian end-to-end analysis framework, and use the resulting data to constrain the spectrum of the cosmic infrared background (CIB; Watts et al. 2024b). The DIRBE instrument observed the full sky in 10 wavelength bands covering 1.25 and 240  $\mu\text{m}$ . By virtue of covering virtually the entire infrared regime, DIRBE is an excellent dust tracer, both originating from the Milky Way and from within the Solar system. Indeed, while DIRBE's original science goal was to detect and characterize the CIB spectrum and fluctuations, the most long-lasting legacy of the survey has arguably been to serve as a unique well-calibrated full-sky tracer of dust emission in the Milky Way (Schlegel et al. 1998; Miville-Deschénes & Lagache 2005; Planck Collaboration X 2016; Sano et al. 2016; Pan-Experiment Galactic Science Group 2025) and zodiacal light emission (e.g., Kelsall et al. 1998; Planck Collaboration XIV 2014; Kondo et al. 2016; San et al. 2024; O'Brien et al. 2025).

One of the many important questions in which the DIRBE data has played a role regards the nature and composition of thermal dust emission in the far-infrared regime, and how it may be modelled most efficiently. Early studies quickly suggested that a single so-called modified blackbody (MBB) spectrum provides a good fit to the thermal dust spectral energy density (SED) for a broad range of frequencies (Reach et al. 1995). An MBB spectrum has three degrees of freedom, namely an overall amplitude (tracing the density of the medium), an effective temperature,  $T$ , and a spectral index,  $\beta$ . To this date, the single-component MBB model plays a key role in both microwave modelling and infrared-based dust studies.

However, it also quickly became clear that the validity of a single MBB spectrum is limited in frequencies. Notably, in a seminal paper Finkbeiner et al. (1999) presented a two-component MBB thermal dust model derived from the *IRAS* 100  $\mu\text{m}$  and DIRBE 100 and 240  $\mu\text{m}$  data that served as a benchmark for the CMB community for more than a decade, and was only superseded by the far more sensitive *Planck* HFI data (Planck Collaboration XI 2014). Since that time, the combination of *Planck*, DIRBE, and *IRAS* measurements have dominated the study of large-scale dust emission at microwave and far-infrared frequencies.

Despite massive efforts developing increasingly more accurate and well-defined models of thermal dust emission, combining theoretical insights with observational constraints (e.g., Draine 2011; Hensley & Draine 2023), many critical questions plague this field to date. Furthermore, the importance of understanding microwave dust emission has only increased in recent years, as the attention of the CMB field has shifted to the search for inflationary gravitational waves through  $B$ -mode polarization constraints (e.g., BICEP2 Collaboration 2018; Ade et al. 2019; LiteBIRD Collaboration et al. 2023). For such experiments, polarized thermal dust emission represents one of the most important contaminants, and major resources are currently being invested in devising both instrumental and data analysis techniques to handle this challenge optimally.

In the current paper, and in two companion papers by Sullivan et al. (2026) and Gjerløw et al. (2026), we revisit the question of how to model thermal dust emission efficiently in light of the currently reprocessed DIRBE data, jointly with archival measurements from *Planck* HFI. Specifically, during the course of the COSMOGLOBE DR2 work, a new four-component MBB model, based on five astrophysical tracers, has emerged as a particularly compact and efficient description. Although a four-component model may at first sight appear as significantly more complicated

**Table 1.** Templates used for each frequency band.

Band	Freq. (GHz)	C II	HI4PI	Gaia	WHAM	CO
<i>Planck</i> 353 GHz	353	x	x	x	x	x
<i>Planck</i> 545 GHz	545	x	x	x	x	x
<i>Planck</i> 857 GHz	857	x	x	x	x	x
DIRBE 240 $\mu\text{m}$	1250	x	x	x	x	x
DIRBE 140 $\mu\text{m}$	2100	x	x	x	x	x
DIRBE 100 $\mu\text{m}$	3000	x	x	x	x	x
DIRBE 60 $\mu\text{m}$	5000	x	x	x	x	x
DIRBE 25 $\mu\text{m}$	12000	x	x			
DIRBE 12 $\mu\text{m}$	25000	x				

than either the standard single-component MBB model adopted by the *Planck* team, or by the two-component MBB model pioneered by Finkbeiner et al. (1999), the key point in our new analysis is that all four components are well traced by well-known dust templates coupled with spatially isotropic SEDs. The number of degrees of freedom per pixel is therefore very small, allowing for a very rigid and compact statistical description.

Four of the five templates in this model are already known to be efficient dust tracers, namely 1) HI4PI H I line emission, tracing molecular gas; 2) Gaia extinction, tracing near-by dust absorption; 3) Dame et al. (2001b) CO line emission, tracing cold dust in star-forming regions; and 4) WHAM H $\alpha$  line emission, tracing hot dust in ionized regions. However, in this paper and its companion papers, we additionally find that ionized carbon emission, as traced by the FIRAS C II 158  $\mu\text{m}$  line emission map, is an excellent tracer of thermal dust emission with a temperature of  $\sim$ 25–30 K. This observation may have far-reaching consequences for future studies and models of dust emission in the microwave and infrared regimes.

In the current paper, we perform a linear regression analysis of *Planck* HFI 353–857 GHz and DIRBE 3.5–100  $\mu\text{m}$  data with this model, which demonstrates the validity of this key finding, even with a minimal set of assumptions. In a follow-up analysis by Sullivan et al. (2026), we perform a Bayesian analysis of *Planck* HFI data with the goal of deriving high-resolution templates of the H I and C II correlated components directly from microwave data. Finally, Gjerløw et al. (2026) applies this novel model to the *COBE*-DIRBE data.

The rest of the paper is organized as follows: in Sect. 2 we discuss the template fitting algorithm and in Sect. 3 the data used in the current paper; finally, in Sect. 4 we present the results from these calculations, before we conclude in Sect. 5.

## 2. Template fitting methodology

As the aim of this paper is mainly to investigate the feasibility of describing thermal dust as a linear combination of components – components that can be reasonably imagined to be associated with the thermal dust in the galaxy – we perform a fitting of such components to existing data *outside* of the COSMOGLOBE framework proper. That is, we here attempt to fit the aforementioned components directly to dust-dominated *Planck* HFI and DIRBE data, and we do this without any joint modelling like the one used in COSMOGLOBE.

In order to perform such a fit, we first assume all components and all data on which we wish to perform the fit are given as

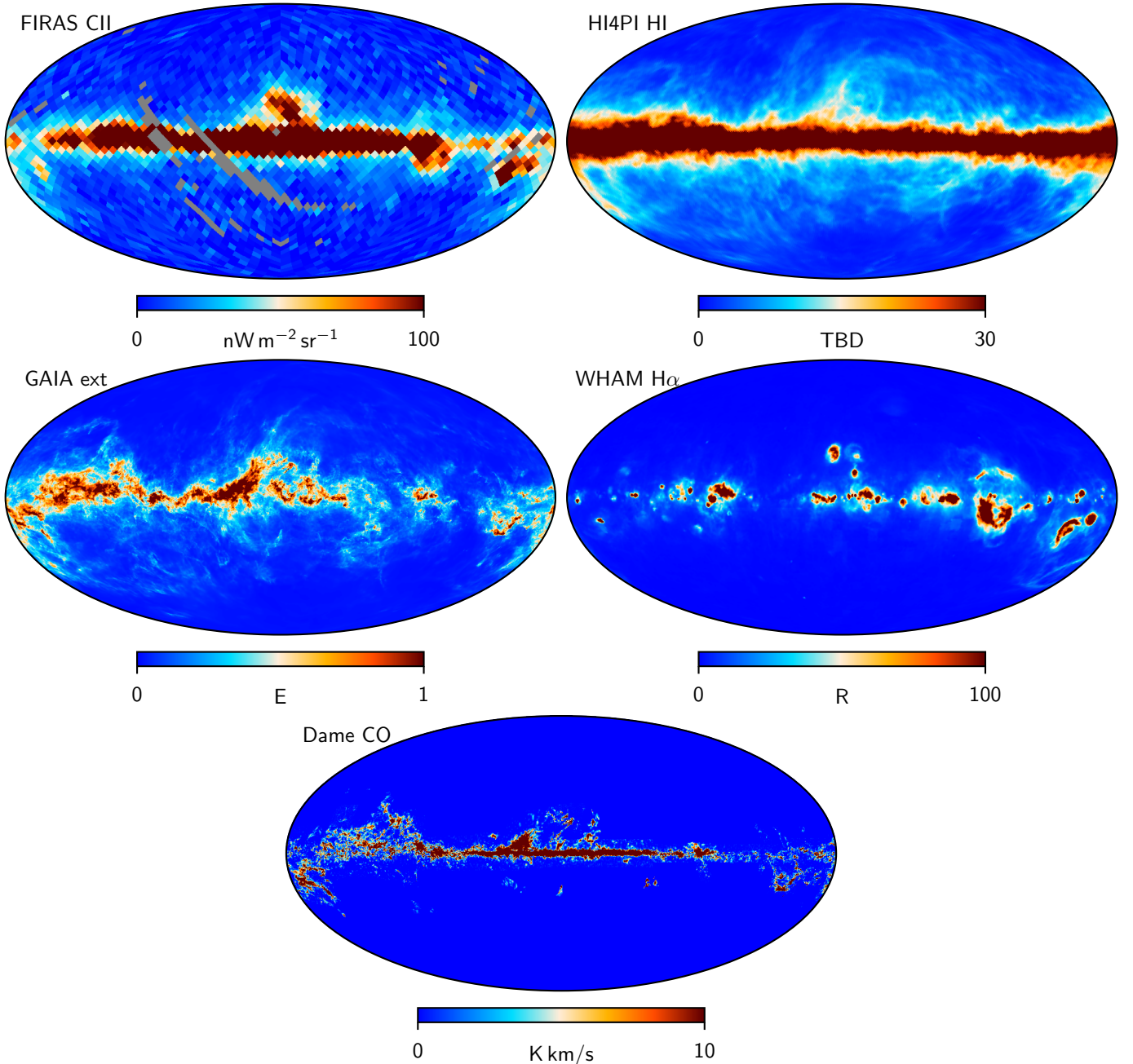


**Fig. 1.** Input maps of each of the following thermal dust tracers (from left to right and top to bottom): C II 158  $\mu\text{m}$  line emission from *COBE*-FIRAS, H I line emission from HI4PI, dust extinction from *Gaia*, H $\alpha$  line emission from WHAM, and CO line emission from Dame et al. (2001b). All maps are smoothed to the FIRAS beam and then used for the low-resolution template fitting at  $N_{\text{side}}=16$ .

HEALPix<sup>1</sup> (Górski et al. 2005; Zonca et al. 2019) maps in the same resolution (see Sect. 3 for more on this). For each data set  $\mathbf{d}_i$  at a given frequency band  $i$  (bold notation here implies a vector of  $n_{\text{pix}}$  HEALPix pixels), the basic data model we employ is

$$\mathbf{d}_i = \sum_c a_{i,c} \mathbf{t}_c + \mathbf{m}_i + \mathbf{n}_i, \quad (1)$$

where the sum over  $c$  runs over  $n_{\text{comp}}$  dust components, each with an amplitude  $a_{i,c}$  and a spatial template  $\mathbf{t}_c$ . In addition, we include a monopole term,  $\mathbf{m}_i$ , and a white noise contribution,  $\mathbf{n}_i$ .

We assume that the data do *not* include CMB, CIB, or zodiacal light contributions, as these are removed through preprocessing; see Sect. 3 for details.

We allow for masking of the data and components, with the only effect being to make each vector in the equation shorter, and  $n_{\text{pix}}$  in what follows is the effective number of pixels after masking.

Given this model, the main goal becomes to find the set of amplitudes  $a_{i,c}$  (and monopole) that jointly minimize the residual

$$\mathbf{r}_i \equiv \mathbf{d}_i - \mathbf{s}_i, \quad (2)$$

where we define  $\mathbf{s}_i$  to be all the terms on the right hand side of Eq. (1) except the white noise term.

<sup>1</sup> <http://healpix.sourceforge.net/>

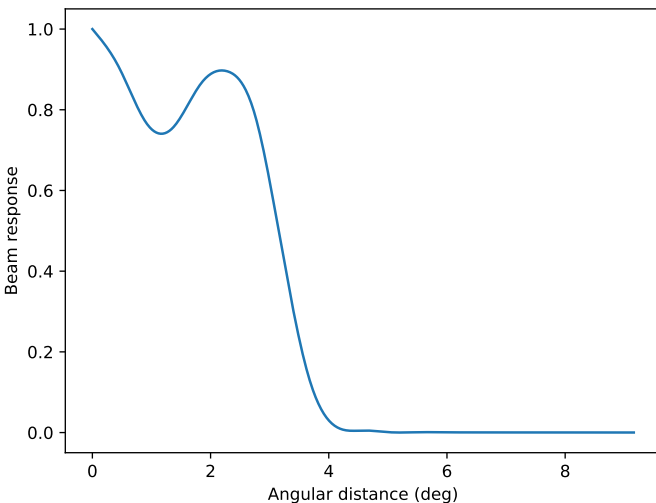


**Fig. 2.** The *COBE*-FIRAS beam, with which all maps in this analysis were smoothed. The beam diameter is around  $7^\circ$  on the sky, which limits this analysis to  $N_{\text{side}}=16$ .

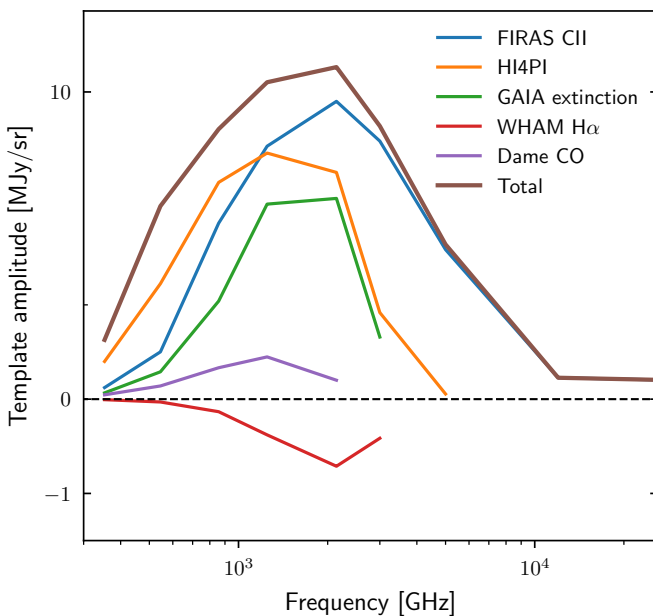


**Fig. 3.** Template amplitudes as a function of frequency for the nine channels used in this analysis, plotted only at the channels where they are fit. The WHAM H $\alpha$  amplitudes are negative because it is an absorptive template.

This kind of minimization for a linear problem has a well-known solution. We annotate our solution vector at each frequency band as  $\mathbf{a}_i$  (which, in this case, is an  $n_{\text{comp}}+1$ -dimensional vector, the extra dimension being due to the monopole contribution), and we can then write

$$\mathbf{a}_i = (\mathbf{T}^T \mathbf{T})^{-1} (\mathbf{T}^T \mathbf{d}), \quad (3)$$

where we define  $\mathbf{T}$  as a  $n_{\text{pix}}$  by  $n_{\text{comp}} + 1$  matrix such that matrix column  $c$  contains component template  $\mathbf{t}_c$  (and the final column is a constant, representing the monopole). Implicit in this way of solving for the amplitudes is the assumption that the noise root mean squared (RMS) is constant from pixel to pixel. At the resolutions used for this analysis, this is a fair assumption, as large-scale instrumental features are dominated by systematic effects

rather than white noise. Solving this equation, the solution vector will then have as its  $n_{\text{comp}}+1$  elements the best-fit amplitudes for each component (and best-fit monopole).

### 3. Data

As, in this paper and its companions, we are mostly concerned with economical dust modelling, we use the most accurate data available in the frequency ranges where dust dominates. More specifically, we use the 353, 545 and 857 GHz frequency bands from *Planck* HFI, as well as the six longest wavelength bands (from 240  $\mu\text{m}$  to 12  $\mu\text{m}$ ) from the DIRBE data.

We use five known or derived dust tracers as component templates: The *COBE*-FIRAS C II observations, the HI4PI neutral hydrogen map, the Dame CO  $J = 1 \rightarrow 0$  map, the WHAM ionized hydrogen map, and a derived map of nearby dust structures based on *Gaia* observations. We note that the fitting procedure described in Sect. 2 does not require that we use the same templates for all data bands, and because some of these five templates are only expected to be relevant at lower frequencies, we will restrict the number of templates used for each band according to Table 1. We provide justification for these restriction in the following sections, on a per-component basis.

We will first describe the DIRBE and *Planck* HFI data sets, before describing the dust tracing templates in more detail, and for which frequencies they are relevant. Finally, we describe the preprocessing and masking steps used for this analysis.

#### 3.1. Frequency maps

##### 3.1.1. DIRBE

The Diffuse InfraRed Explorer (DIRBE), whose main goal was the mapping of the CIB, was part of the *COBE* satellite (Boggess et al. 1992; Silverberg et al. 1993), and measured the sky in ten frequency bands, from 1  $\mu\text{m}$  to 240  $\mu\text{m}$ .

In this analysis, we started from the  $N_{\text{side}} = 512$  maps created with the procedure described in Watts et al. (2024a) from the DIRBE CIO (Calibrated Individual Observations). The shortest-wavelength features of thermal dust are the polycyclic aromatic hydrocarbon features, which are expected to be detectable in the spectrum down to a few microns (Hensley & Draine 2021). We, therefore, include the eight longest wavelength bands of DIRBE, ranging from 240  $\mu\text{m}$  to 3.5  $\mu\text{m}$ .

##### 3.1.2. Planck HFI

The *Planck* High Frequency Instrument (HFI; Planck Collaboration III 2020) observed the sky in six frequency channels from 100 GHz to 857 GHz, with the primary purpose of characterizing temperature fluctuations in the CMB to unprecedentedly small scales. As it also was able to target the far-infrared sky, it is able to shed some light on the dust population of the sky (Planck Collaboration Int. XVII 2014; Planck Collaboration X 2016; Planck Collaboration III 2020).

Since this work is primarily concerned with dust modeling, we attempt to avoid contamination from (especially) the CMB signal, which dominates at the lower *Planck* frequencies. To that end, we use only the HFI data from 353 to 857 GHz. All of the input frequency maps are taken from the *Planck* PR4 data release (Planck Collaboration LVII 2020).

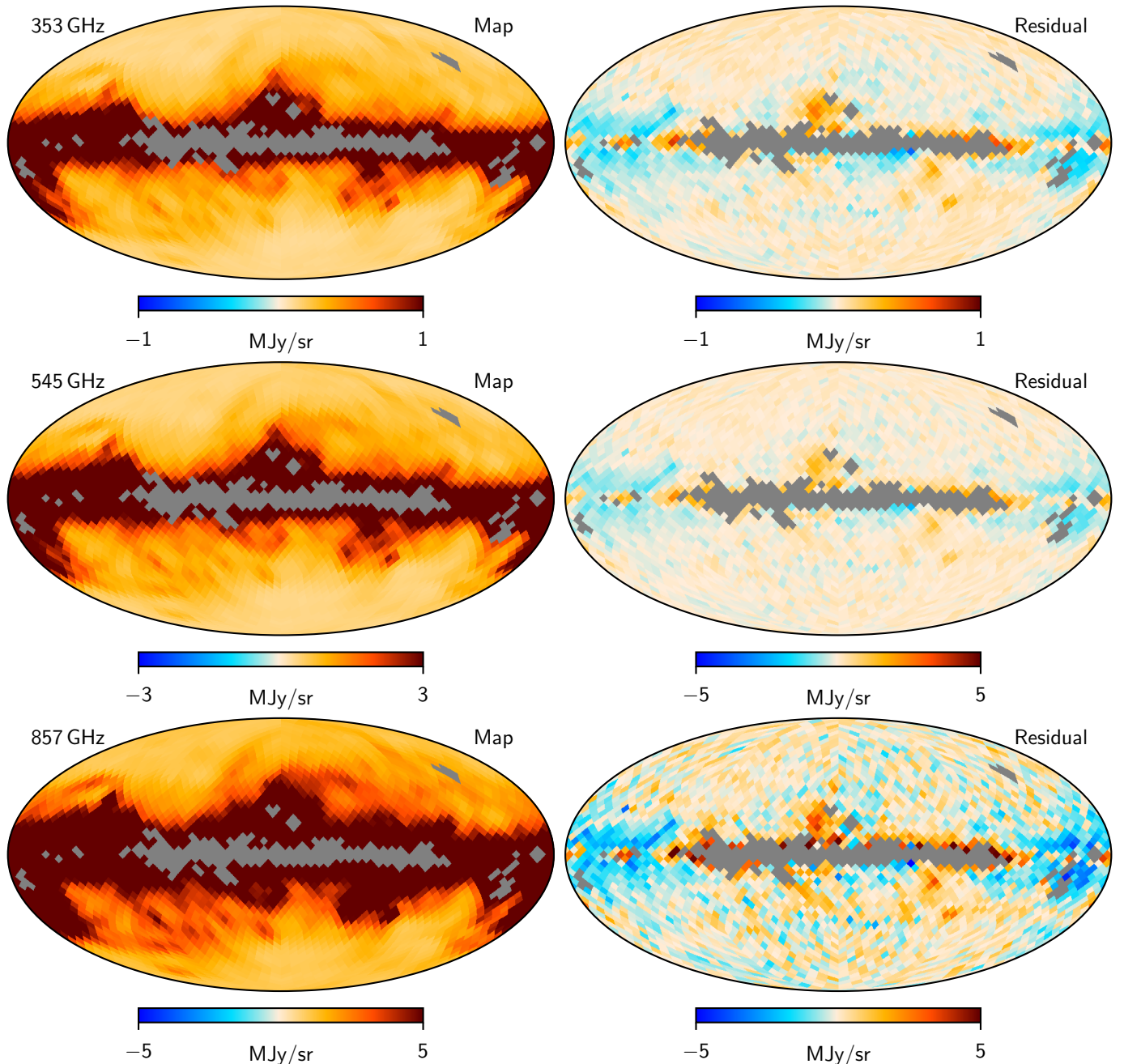


**Fig. 4.** Comparison between full (left column) and template cleaned (right) maps for the three dust-dominated *Planck* HFI channels. The grey pixels are masked by the common analysis mask. All maps are convolved with the FIRAS beam.

### 3.2. Thermal dust tracers

In this work, we take from legacy and state-of-the-art data sets in order to find reliable maps for the tracers of thermal dust emission we are looking for. Below, we describe each of these data sets in turn, and in Fig. 1, we show the input maps used for the template fitting.

#### 3.2.1. Ionized carbon — COBE-FIRAS C II

The *COBE*-FIRAS instrument is the only full-sky spectrometric survey in the radio and infrared electromagnetic wavelengths, and as such, it provides the best full-sky measurement of spectral line emission. The  $157.7\text{ }\mu\text{m}$  C II line emission has previously

been recognized as a gas tracer; here, we investigate its potential as a tracer of interstellar dust.

We use the *COBE*-FIRAS C II map, available on the LAMBDA website.<sup>2</sup> As this is the lowest-resolution map in the analysis, we do not perform any preprocessing on the map before using it as a template.

#### 3.2.2. Neutral hydrogen – HI4PI

The HI4PI HI survey (HI4PI Collaboration: et al. 2016) is a full-sky survey of the 21 cm hydrogen line, performed by a combination of data from EBHIS and GASS. The 21 cm line has been used as a tracer for dust structures (Planck Collaboration XXIV

<sup>2</sup> [lambda.gsfc.nasa.gov](http://lambda.gsfc.nasa.gov)

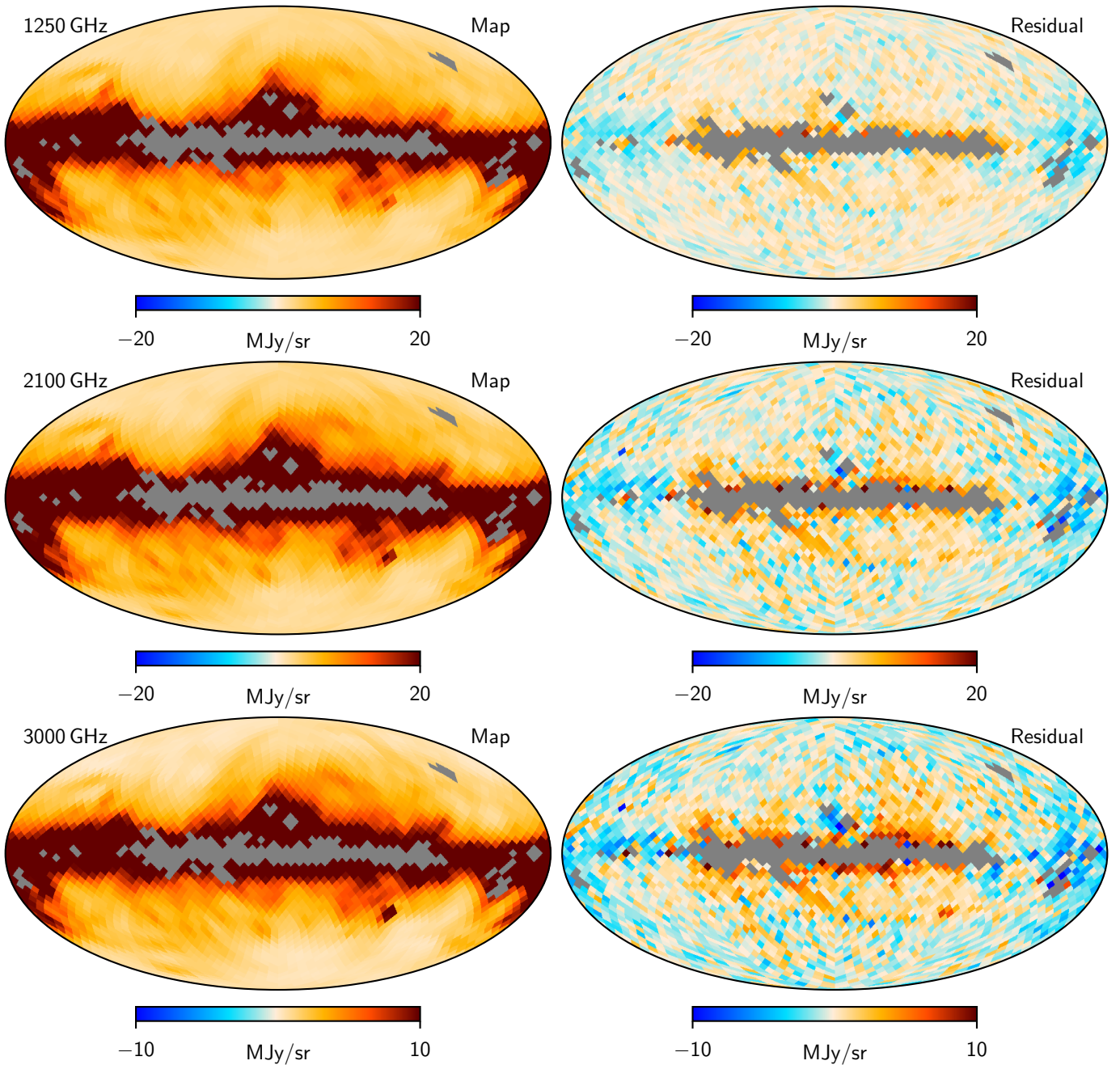


**Fig. 5.** Same as Fig. 4 but for the three lowest frequency DIRBE channels ( $240\mu\text{m}$  -  $100\mu\text{m}$ ).

2011), and is typically associated with low-intensity regions of the sky (as it requires the hydrogen to not be ionized, and be in its lowest energy state).

### 3.2.3. Nearby dust through extinction – Gaia

One source of important information about the 3-dimensional structure of dust is starlight extinction. By comparing expected stellar spectra with observed ones, Edenhofer et al. (2024) was able to reconstruct such dust structures up to a distance of (TBD), represented by a series of maps for each distance bin. Using the accompanying software, we integrated these maps out to their furthest distance, which still represents relatively close dust structures, galactically speaking, and we use this as a template for nearby dust structures. The choice of the distance cut is

driven more by the available Edenhofer maps than any physical considerations; still, in this work, this seems to be the best way of utilizing the available additional information about the dust morphology that these maps represent.

### 3.2.4. Ionized hydrogen – WHAM

The Wisconsin H-Alpha Mapper (WHAM) (Haffner et al. 2003b, 2010) surveyed the intensity of the  $\text{H}\alpha$  line over the whole sky, with a resolution of 1 degree, and a velocity resolution of 12 km/s. This line is typically associated with higher energy regions, as it is most commonly emitted from hydrogen atoms recombining after ionization. The WHAM  $\text{H}\alpha$  map was used in *Planck* as a tracer of nearby free-free emission (morphologically, it is clearly tracing “globules” of activity which, both

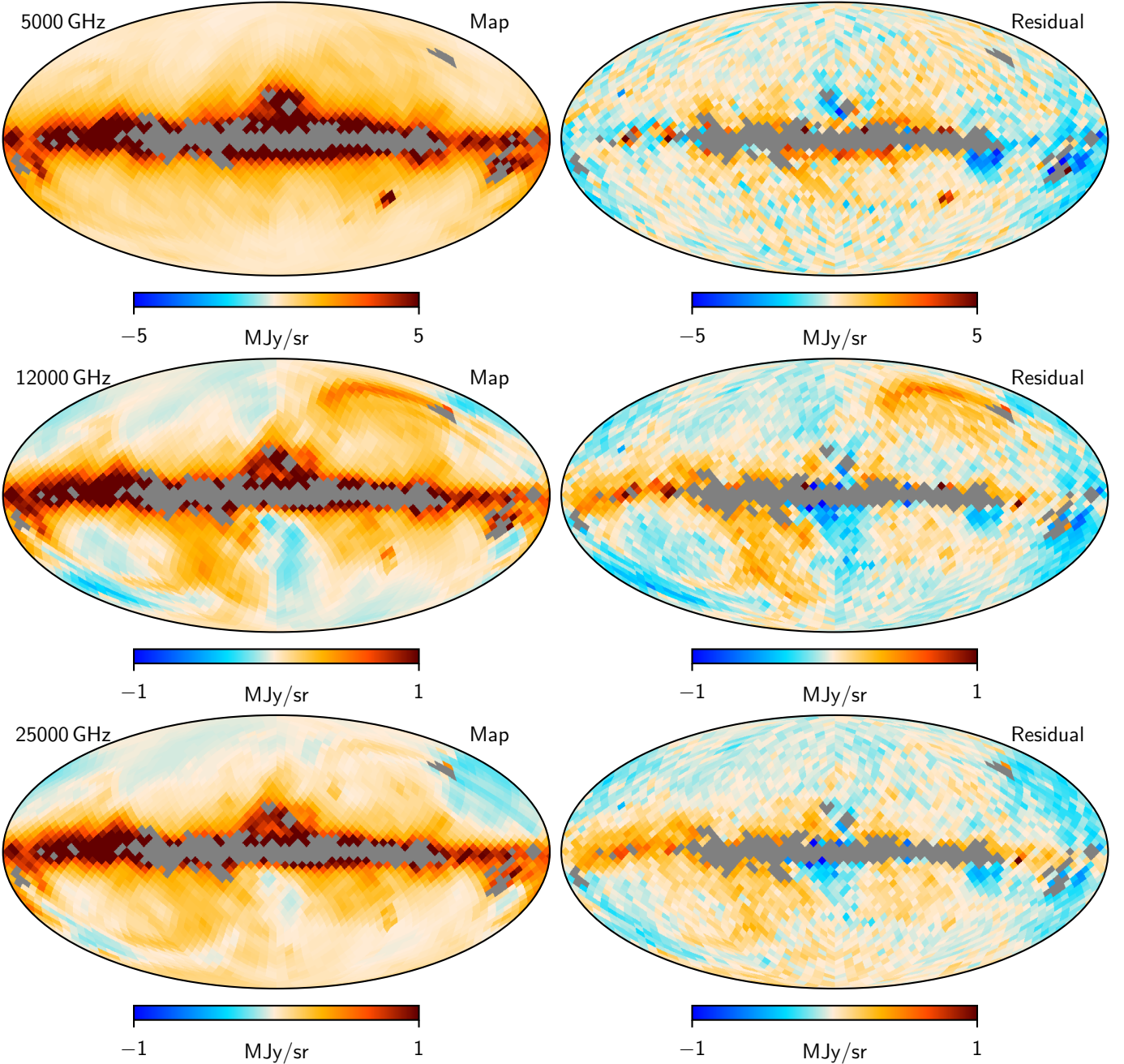


**Fig. 6.** Same as Fig. 4 but for the three intermediate frequency DIRBE channels ( $60\mu\text{m}$  -  $12\mu\text{m}$ ).

by virtue of their size on the sky and the fact that the galactic center is not discernible, must be relatively close).

### 3.2.5. Carbon monoxide – Dame CO $J = 1\text{-}0$

Dame et al. (2001b) surveyed about 45% of the sky for the  $J = 1\text{-}0$  CO line within 30 degrees of the Galactic equator. As dust is expected to be located in molecular clouds, the CO line would be a natural tracer for such dust populations.

### 3.3. Low-resolution preprocessing

The template fitting procedure described in Sect. 2 requires all maps to be smoothed to a common resolution – if not, the extra degrees of freedom at smaller scales in some of the maps and

templates might bias the fit at larger scales. Out of all the data and templates used in this analysis, the *COBE*-FIRAS C II map is the one with the lowest native resolution. We therefore convolve all maps with the *COBE*-FIRAS beam, shown in Fig. 2, taking into account the drift along the Ecliptic (e.g., Odegard et al. 2019), and we repixelate all maps to a HEALPix resolution of  $N_{\text{side}} = 16$ .

### 3.4. Processing mask

The FIRAS CII map in particular contains systematic effects, which we mask in this analysis. In addition, due to the complexity of the galactic center, as well as certain high-activity complexes (TBD), we mask these as well.

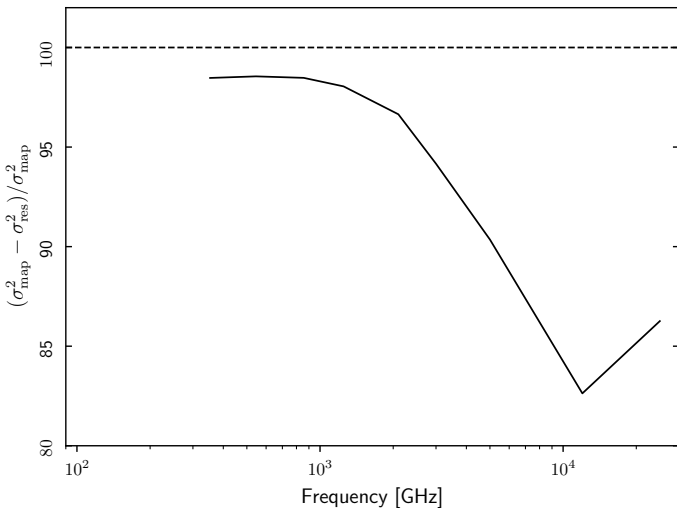


**Fig. 7.** Efficiency of the dust model at describing the data at each frequency. We subtract the squared residuals from the squared map, and normalize by the amplitude of the map. The five component template-based dust model is able to recover more than 80% of the total map power at all frequencies, including those with known residual zodiacal contamination like  $25\mu\text{m}$ .

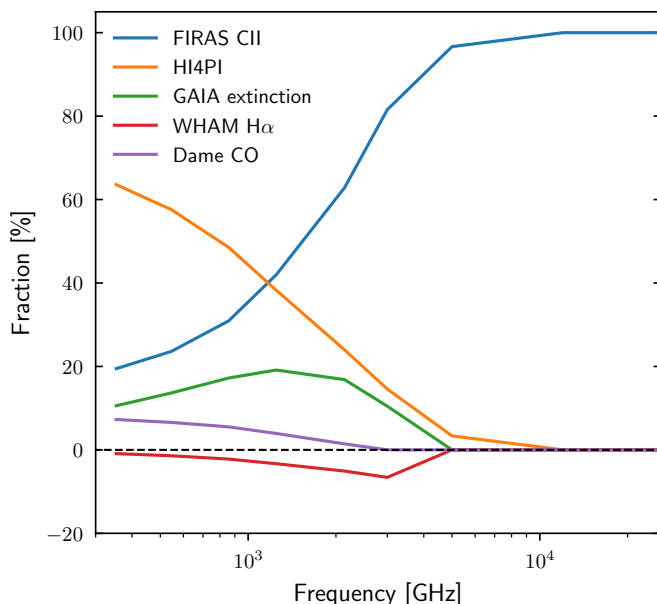


**Fig. 8.** The relative template amplitudes at each frequency, showing the power contribution of each component as a percentage of the combined model amplitude.

## 4. Results

### 4.1. Template amplitude fits

The fit template amplitudes per frequency band are shown in Fig. 3. As is evident, the spectra of all templates show a characteristic bump, which is the expected behavior of modified blackbody SEDs with temperatures in the typical thermal dust temperature range (see below for actual temperature estimations of these spectra).

We also see that the  $\text{H}\alpha$  component has a negative SED, showing that it indeed functions as a dust extinction template.

### 4.2. Model efficiency and goodness-of-fit

In Figs. 4 to 6, we show a comparison between the original data (left columns) and the template cleaned maps (right columns). Clearly, the template fitting performs well on all frequencies, leaving residual signals that are associated with high-activity regions of the Milky Way (especially evident in the 857 GHz and 3000 GHz residuals), as well as unmodelled zodiacal emission from the Solar System (evident in the two highest frequency maps). Overall, a by-eye survey seems to indicate that the template fitting is an efficient procedure for accounting for most of the dust.

In order to quantify the degree to which this impression bears out in practice, in Fig. 7 we construct a measure of the amount of signal that is “explained” by the template fit. It is constructed by taking the RMS of the pixel values in the original map, as well as those of the residual map after template subtraction, and subtracting these values from each other, normalizing the value by the original RMS. We see that the fraction of unexplained RMS left in the map ranges from about 2% (for the lower frequencies) to around 15%, and we note that the only two maps that have more than 5% of unexplained RMS are the two maps where the imprint of remaining zodiacal light is the strongest.

### 4.3. Modified blackbody fits

In Fig. 9, we fit the following modified blackbody model to the template fitting SEDs:

$$s(\nu) = A \frac{\nu^{\beta+3}}{\exp(\frac{h\nu}{k_b T}) - 1}. \quad (4)$$

Here,  $A$  is an arbitrary scaling factor,  $T$  is the blackbody temperature, and  $\beta$  is the spectral index of the modified blackbody. It is especially interesting to compare the two strongest SEDs – those associated with the CII template and the HI template, respectively, as we see that they correspond to significantly different temperatures. Thus, the dust that the CII template traces morphologically (which we *a priori* would assume to be associated with high-energy regions because of the high transitional energy of this line) also seems to exhibit a high intrinsic temperature.

Similarly, we may draw the opposite conclusions regarding the dust traced by the HI template: As expected, this dust exhibits a much lower temperature, consonant with the picture of it being located in low-intensity regions.

The *Gaia* extinction template exhibits an even lower temperature, but it is also modified by a significantly steeper spectral index, indicating a higher degree of absorption at the lower frequencies.

The Dame CO template is the coldest of all the components, while still exhibiting a relatively steep spectral index, which might indicate that this dust emission originates from cold star-forming regions.

The WHAM  $\text{H}\alpha$  template exhibits the steepest spectrum of all the components, consistent with it being correlated with regions of high activity.

## 5. Conclusions

In this paper, we have fit five templates based on pre-existing data sets which might be expected to correlate to dust in some way to frequency maps from *Planck* HFI and DIRBE: A CII template based on FIRAS data; a HI template from the HI4PI survey;

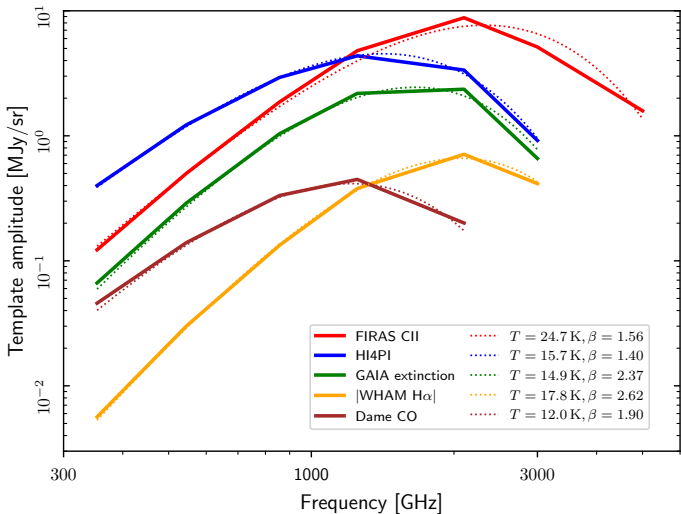


**Fig. 9.** Comparison between template fit amplitudes (solid lines, reproduced from Fig. 3) with best-fit modified blackbody models (dotted lines), in the thermal regime for each component. The best-fit MBB temperatures and  $\beta$ s for each curve are listed in the figure legend.

a “nearby dust” template constructed from integrated *Gaia* extinction maps made by Edenhofer et al., the Dame CO template; and a WHAM H $\alpha$  template.

We fit these to data (downgraded to the FIRAS beam) from *Planck* HFI and DIRBE, from 353 GHz to 12  $\mu$ m, where thermal dust emission is one of the main sources of foreground contamination. We show that this template fit is both able to account for at least 95% of the dust RMS for all but the two highest frequency bands, and that the resulting SEDs follow modified blackbody curves with clearly defined temperatures and spectral indices.

In particular, we find that the two most dominant components – traced by the CII and HI templates – exhibit similar spectral indices, but very different blackbody temperatures (24.7 and 15.7 K, respectively). Thus, these templates trace dust populations that originate in significantly different environments. The H $\alpha$  template traces dust that is mainly making its presence known through extinction – the steep spectral index for this template is consistent with the assumption that this dust is mostly located in nearby high-activity regions.

This analysis shows that it is possible to vastly reduce the complexity of the challenge of thermal dust modelling: Instead of operating with models that have several free parameters per pixel, this approach shows that it should be possible to reduce the degrees of freedom quite extensively by assuming a limited number of populations of dust extending across the sky with common physical parameters, and that such populations can helpfully be informed by utilizing data that is assumed to trace physical processes and environmental conditions.

A natural question arising from this analysis is whether the method proposed here also applies to polarized dust emission, and this question will be the subject of a future analysis. If this turns out to be the case, it would have a significant impact on the feasibility of modelling polarized dust emission for future CMB experiments, which are dependent on accurate modelling of polarized foregrounds to reach the sensitivities required for their science goals (in particular, the detection of  $r$ ).

**Acknowledgements.** We thank Richard Arendt, Tony Banday, Johannes Eskilt, Dale Fixsen, Ken Ganga, Paul Goldsmith, Shuji Matsuura, Sven Wedemeyer, Janet Weiland and Edward Wright for useful suggestions and guidance. The

current work has received funding from the European Union’s Horizon 2020 research and innovation programme under grant agreement numbers 819478 (ERC; COSMOGLobe), 772253 (ERC; bItS2cosmology), 101165647 (ERC, ORIGINS), 101141621 (ERC, COMMANDER), and 101007633 (MSCA; CMBInFLATE). This article reflects the views of the authors only. The funding body is not responsible for any use that may be made of the information contained therein. This research is also funded by the Research Council of Norway under grant agreement number 344934 (YRT; COSMOGLobeHD). Some of the results in this paper have been derived using healpy (Zonca et al. 2019) and the HEALPix (Górski et al. 2005) packages. We acknowledge the use of the Legacy Archive for Microwave Background Data Analysis (LAMBDA), part of the High Energy Astrophysics Science Archive Center (HEASARC). HEASARC/LAMBDA is a service of the Astrophysics Science Division at the NASA Goddard Space Flight Center. This publication makes use of data products from the Wide-field Infrared Survey Explorer, which is a joint project of the University of California, Los Angeles, and the Jet Propulsion Laboratory/California Institute of Technology, funded by the National Aeronautics and Space Administration. This work has made use of data from the European Space Agency (ESA) mission *Gaia* (<https://www.cosmos.esa.int/gaia>), processed by the *Gaia* Data Processing and Analysis Consortium (DPAC, <https://www.cosmos.esa.int/web/gaia/dpac/consortium>). Funding for the DPAC has been provided by national institutions, in particular the institutions participating in the *Gaia* Multilateral Agreement. We acknowledge the use of data provided by the Centre d’Analyse de Données Etendues (CADE), a service of IRAP-UPS/CNRS (<http://cade.irap.omp.eu>, Paradis et al. 2012). This paper and related research have been conducted during and with the support of the Italian national inter-university PhD programme in Space Science and Technology. Work on this article was produced while attending the PhD program in PhD in Space Science and Technology at the University of Trento, Cycle XXXIX, with the support of a scholarship financed by the Ministerial Decree no. 118 of 2nd March 2023, based on the NRRP - funded by the European Union - NextGenerationEU - Mission 4 “Education and Research”, Component 1 “Enhancement of the offer of educational services: from nurseries to universities” - Investment 4.1 “Extension of the number of research doctorates and innovative doctorates for public administration and cultural heritage” - CUP E66E23000110001.

## References

- Ade, P., Aguirre, J., Ahmed, Z., et al. 2019, *J. Cosmology Astropart. Phys.*, 2019, 056
- BICEP2 Collaboration. 2018, *Phys. Rev. Lett.*, 121, 221301
- Boggess, N. W., Mather, J. C., Weiss, R., et al. 1992, *ApJ*, 397, 420
- Dame, T. M., Hartmann, D., & Thaddeus, P. 2001a, *ApJ*, 547, 792
- Dame, T. M., Hartmann, D., & Thaddeus, P. 2001b, *ApJ*, 547, 792
- Draine, B. T. 2011, *Physics of the Interstellar and Intergalactic Medium* (Princeton University Press)
- Edenhofer, G., Zucker, C., Frank, P., et al. 2024, *A&A*, 685, A82
- Finkbeiner, D. P., Davis, M., & Schlegel, D. J. 1999, *ApJ*, 524, 867
- Gjerløw et al. 2026, *A&A*, in preparation [[arXiv:20xx.xxxxx](https://arxiv.org/abs/20xx.xxxxx)]
- Górski, K. M., Hivon, E., Banday, A. J., et al. 2005, *ApJ*, 622, 759
- Haffner, L. M., Reynolds, R. J., Babler, B. L., et al. 2016, in *American Astronomical Society Meeting Abstracts*, Vol. 227, American Astronomical Society Meeting Abstracts #227, 347.17
- Haffner, L. M., Reynolds, R. J., Madsen, G. J., et al. 2010, in *American Astronomical Society Meeting Abstracts*, Vol. 215, American Astronomical Society Meeting Abstracts #215, 415.28
- Haffner, L. M., Reynolds, R. J., Tufte, S. L., et al. 2003a, *ApJS*, 149, 405
- Haffner, L. M., Reynolds, R. J., Tufte, S. L., et al. 2003b, *ApJS*, 149, 405
- Hauser, M. G., Arendt, R. G., Kelsall, T., et al. 1998, *ApJ*, 508, 25
- Hensley, B. S. & Draine, B. T. 2021, *ApJ*, 906, 73
- Hensley, B. S. & Draine, B. T. 2023, *ApJ*, 948, 55
- HI4PI Collaboration; Ben Bekhti, N., Flöer, L., et al. 1998, *ApJ*, 508, 44
- Kelsall, T., Weiland, J. L., Franz, B. A., et al. 1998, *ApJ*, 508, 44
- Kondo, T., Ishihara, D., Kaneda, H., et al. 2016, *AJ*, 151, 71
- LiteBIRD Collaboration, Ally, E., Arnold, K., et al. 2023, *Progress of Theoretical and Experimental Physics*, 2023, 042F01
- Miville-Deschénes, M.-A. & Lagache, G. 2005, *ApJS*, 157, 302
- O’Brien, R., Arendt, R. G., Windhorst, R. A., et al. 2025, arXiv e-prints, [arXiv:2510.18231](https://arxiv.org/abs/2510.18231)
- Odegard, N., Weiland, J. L., Fixsen, D. J., et al. 2019, *ApJ*, 877, 40
- Pan-Experiment Galactic Science Group. 2025, *The Astrophysical Journal*, 991, 23
- Paradis, D., Dobashi, K., Shimoikura, T., et al. 2012, *A&A*, 543, A103
- Planck Collaboration XXIV. 2011, *A&A*, 536, A24
- Planck Collaboration XI. 2014, *A&A*, 571, A11
- Planck Collaboration XIV. 2014, *A&A*, 571, A14
- Planck Collaboration X. 2016, *A&A*, 594, A10

- Planck Collaboration III. 2020, A&A, 641, A3  
Planck Collaboration Int. XVII. 2014, A&A, 566, A55  
Planck Collaboration LVII. 2020, A&A, 643, A42  
Reach, W. T., Dwek, E., Fixsen, D. J., et al. 1995, ApJ, 451, 188  
San, M. et al. 2024, A&A, in preparation [arXiv:20xx.xxxxx]  
Sano, K., Kawara, K., Matsuura, S., et al. 2016, ApJ, 818, 72  
Schlegel, D. J., Finkbeiner, D. P., & Davis, M. 1998, ApJ, 500, 525  
Silverberg, R. F., Hauser, M. G., Boggess, N. W., et al. 1993, in Society of Photo-  
Optical Instrumentation Engineers (SPIE) Conference Series, Vol. 2019, In-  
frared Spaceborne Remote Sensing, ed. M. S. Scholl, 180–189  
Sullivan et al. 2026, A&A, in preparation [arXiv:20xx.xxxxx]  
Watts, D., Galloway, M., Gjerlow, E., et al. 2024a, A&A, submitted  
[arXiv:2408.10952]  
Watts, D. et al. 2024b, A&A, in preparation [arXiv:2406.01491]  
Zonca, A., Singer, L., Lenz, D., et al. 2019, Journal of Open Source Software, 4,  
1298